RSC Advances

PAPER

View Article Online
View Journal | View Issue

Cite this: *RSC Adv.*, 2015, **5**, 51900

Morphology-dependent performance of $Mg_3Al–CO_3$ layered double hydroxide as a nanofiller for polypropylene nanocomposites

Lei Qiu,[a] Yanshan Gao,[a] Xingru Yan,[b] Jiang Guo,[b] Ahmad Umar,[cd] Zhanhu Guo[b] and Qiang Wang*[a]

Received 30th April 2015
Accepted 5th June 2015

DOI: 10.1039/c5ra07911j

www.rsc.org/advances

In this contribution, the morphology-dependent performance of $Mg_3Al–CO_3$ layered double hydroxide (LDH) as a nanofiller for polypropylene (PP) was evaluated for the first time. Three types of PP nanocomposites with 0-dimensional spherical, 2-dimensional plate-like, and 3-dimensional flower-like $Mg_3Al–CO_3$ LDHs as nanofillers were prepared using a solvent mixing method. The influence of morphology as well as the loading of LDHs on the thermal stability, flame retardancy, and rheological behaviors of the PP/LDH nanocomposites was then systematically investigated. The results showed that the thermal stability was significantly improved after incorporating LDH nanoparticles. For instance, the $T_{0.5}$ of the 13.0 wt% PP/plate-like LDH nanocomposite was increased by 61 °C compared to that of pure PP. The addition of $Mg_3Al–CO_3$ LDHs can enhance the flame retardant performance of PP as well, and the efficiency was dependent on both the morphology and loading of LDH. The influence on the storage modulus (G') and loss modulus (G'') of PP was observed to follow the order of spherical > plate-like > flower-like. This work demonstrated that more attention should be paid to the influence of LDH morphology for the future design of the polymer/LDH nanocomposites.

1. Introduction

With the rapid development of urbanization, polymer-based materials have been recognized as one of the key components in many important applications owing to their outstanding physical and chemical properties. Polypropylene (PP) is one of the most widely used polymers for the preparation of nanocomposites due to its ready availability, excellent processability, and relatively low cost.[1–5] It is also one of the most widely used commodity thermoplastics, which has excellent physical properties, such as high stiffness and tensile strength.[6,7] However, one severe problem with many polymers including PP is that they are highly flammable and can produce large amounts of toxic smoke during combustion, which possess a great threat to human safety and significantly restrict their applications in many areas.[8,9] In order to solve this problem, effective methods are needed to add compatible nano-sized flame retardant fillers into polymer matrices.[10]

In recent years, polymer/layered double hydroxide (LDH) nanocomposites have drawn more attention among the polymer/inorganic filler nanocomposites.[11–13] LDHs are a class of ionic lamellar compounds made up of positively charged brucite-like layers with an interlayer region containing charge compensating anions and solvation molecules.[14,15] These materials have received increasing attention due to their many applications as precursors to CO_2 adsorbents,[16–20] catalysts,[21,22] thermal stabilizers,[23,24] IR absorbers,[25,26] UV absorbers,[27–29] and nanofillers in polymer/LDH nanocomposites.[30–34] In general, LDHs might have both the advantages of aluminium hydroxide and magnesium hydroxide flame retardant, and can possibly overcome the shortcomings of individual component. Particularly, LDHs are used widely with the major advantages of flame retardant, smoke inhibition, filled function, non-toxic and so on. Until now, many kinds of LDHs have been reported as nanofillers in polymer nanocomposites. For example, LDHs with different cationic compositions such as Mg–Al,[35–37] Zn–Al,[38,39] and Mg–Zn–Al LDHs[40,41] have been proven to be good flame retardant materials, and both the thermal stability and the rheological behaviors can be enhanced as well. In the meantime, four different inorganic anions (CO_3^{2-}, NO_3^-, Cl^- and SO_4^{2-}) intercalated Mg_3Al or Zn_2Al LDHs as nanofillers prepared by using a solvent mixing method were reported, and the thermal stability and flame retardancy were significantly improved. The influence of interlayer inorganic anions on the

[a]College of Environmental Science and Engineering, Beijing Forestry University, 35 Qinghua East Road, Haidian District, Beijing 100083, P. R. China. E-mail: qiang.wang.ox@gmail.com; qiangwang@bjfu.edu.cn; Tel: +86 13699130626

[b]Integrated Composites Laboratory (ICL), Department of Chemical and Biomolecular Engineering, University of Tennessee, Knoxville, TN 37996, USA

[c]Department of Chemistry, College of Science and Arts, Najran University, Najran-11001, Kingdom of Saudi Arabia

[d]Promising Centre for Sensors and Electronic Devices (PCSED), Najran University, Najran-11001, Kingdom of Saudi Arabia

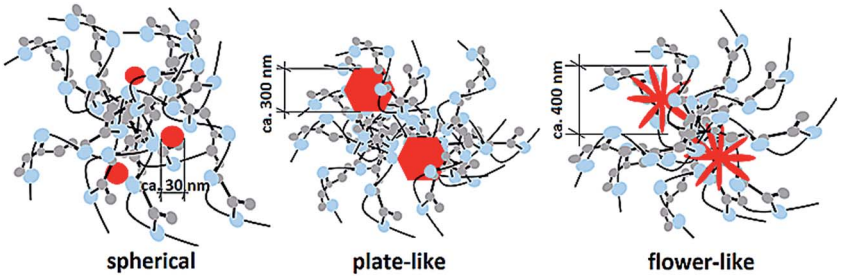

Fig. 1 The schematic structures of the proposed three types of polymer/Mg_3Al–CO_3 LDH nanocomposites. The long-chain molecules represent PP (C atoms (light blue), and H atoms (grey)), and the red nanoparticles represent the LDH nanofillers.

rheological behaviors of PP and HDPE was then systematically compared as well.[42,43]

In addition to the effect of the chemical composition of LDHs, the influence of their morphology is also of great interest. However, mainly due to the difficulty in controlling the morphology of LDHs, such kind of investigation has not been reported yet. In this contribution, we successfully synthesized three types of Mg_3Al–CO_3 LDHs with different morphologies including 0-dimensional spherical nanoparticle, 2-dimensional plate-like particle, and 3-dimensional flower-like particle, and systematically investigated their influence on the thermal, flame retardant, and rheological behaviors for the first time. In order to prevent the agglomeration of LDHs nanoparticles, the PP/LDHs nanocomposites were prepared using a newly developed solvent mixing method.[34] The Mg_3Al–CO_3 LDH was first treated with acetone to improve the miscibility between the typically hydrophobic polymer and the hydrophilic LDHs.[7] Another benefit of employing a solvent-based synthesis method is that it can skip the drying the step of LDH, which consequently preventing the severe aggregation of LDH nanoparticles.[44] Fig. 1 illustrates the obtained three types of different polymer/Mg_3Al–CO_3 LDH nanocomposites. This work is not only important for the future preparation and application of PP/LDH nanocomposites, but also helpful for the understanding of the mechanism of LDHs as multifunctional nanofillers for polymers.

2. Experimental

2.1 Synthesis of LDHs and PP/LDH nanocomposites

The flower-like Mg_3Al–CO_3 LDH was prepared using co-precipitation method with a constant pH of 10. In brief, a 50 ml solution containing 9.6 g Mg $(NO_3)_2 \cdot 6H_2O$ (0.0375 mol) and 4.7 g Al $(NO_3)_3 \cdot 9H_2O$ (0.0125 mol) was added drop-wise to another 50 ml solution containing 2.65 g Na_2CO_3 (0.025 mol), in the meantime the pH of the precipitation solution was strictly controlled at *ca.* 10 using a NaOH (4 M) solution. The resulting mixture was aged at room temperature for 12 h with continuous stirring. The spherical Mg_3Al–CO_3 LDH was synthesized similarly, with an only exception that the pH of the precipitation solution was adjusted to *ca.* 12. The plate-like Mg_3Al–CO_3 LDH can be synthesized with the same pH as the spherical one, but the obtained LDH was further hydrothermally treated at 150 °C for 3 days. All the obtained LDHs were washed with H_2O until pH = 7. The samples were further washed with acetone intensively. Regarding to the synthesis of LDHs, more details can be found in our previous report.[18] For the preparation of PP/LDH nanocomposites, the acetone washed slurries were directly used without drying. Finally all samples were dried in an oven at 65 °C for overnight.

PP/Mg_3Al–CO_3 LDH nanocomposites were prepared using a solvent mixing method. 5 g PP (molecular weight *ca.* 300000), the acetone washed LDH slurry prepared above, and 100 ml xylene were charged into a 250 ml round bottom flask. The amounts of LDHs corresponding to the final nanocomposites were controlled to be 13.0, 16.7, 23.1, and 28.6 wt%, respectively. The mixture was refluxed at approximately 140 °C for 2 h. After the completion of the reflux process, the hot xylene solution containing the dissolved PP and highly dispersed LDH nanoparticles was poured into 100 ml hexane (also called the solvent extraction method). The obtained PP/LDH nanocomposites were collected by filtration and dried under vacuum.

2.2 Characterization of LDHs and PP/LDH nanocomposites

XRD patterns were recorded on a Shimadzu XRD-7000 diffractometer with Cu Kα radiation. The accelerating voltage was set at 40 kV with 30 mA current (λ = 1.542 Å). The diffraction patterns were obtained in the range of 5–70° with a scanning rate of 5° min^{-1} and a slit size of 1°. SEM analysis was performed on a JEOL JSM 6700F scanning microscope with an accelerating voltage of 5.0 kV, powder samples were spread on carbon tape (or silicon wafer) adhered to a SEM stage. Before observation, the samples were sputter coated with a thin platinum layer to prevent charging and to improve the image quality. TEM analysis was performed on a JEOL JEM-1010 microscope with an accelerating voltage of 80 kV, samples were dispersed in ethanol by sonication and then cast onto copper TEM grids coated with a lacey carbon film.

2.3 Thermal stability, flame retardant and rheological property of PP/LDH nanocomposites

The thermal stability of all samples was evaluated using TGA (TGAQ50, TA Instruments-Waters LLC), which was carried out with a heating rate of 10 °C min^{-1} and an air flow rate of 50 ml min^{-1} from 25 to 600 °C. Micro-scale combustion calorimeter

(Model MCC-2, Govmark Organization, Inc.) was used to investigate the combustion property of the synthesized PP and its nanocomposites. For these tests, about 5 mg of sample was heated to 750 °C with a heating rate of 1 °C s^{-1} in a stream of N_2 (80 cm^3 min^{-1}). The volatile, anaerobic thermal degradation products in the N_2 gas stream were mixed with a stream containing 20% O_2 and 80% N_2 (20 cm^3 min^{-1}) prior to entering a 900 °C combustion furnace. The heat release rate (HRR) in W g^{-1} (calculated from the oxygen depletion measurements), heat release capacity (HRC) in J g^{-1} K^{-1} (obtained by dividing the sum of the peak HRR by the heating rate in K s^{-1}), and the total heat release (THR) in kJ g^{-1} (given by integrating the HRR curve) of samples could be obtained from these tests. The melt rheological behaviors of pure PP and its nanocomposites were studied using a TA Instruments AR 2000ex Rheometer. An environmental test chamber (ETC) steel parallel-plate geometry (25 mm in diameter) was used to perform the measurement at 200 °C when PP was in the melt state. The frequency sweep was from 100 to 0.1 Hz in the linear viscoelastic (LVE) range (strain 1%) under a N_2 atmosphere to prevent the oxidation of PP.

3. Results and discussion

3.1 Characterization of LDHs and PP/LDH nanocomposites

The synthesized Mg_3Al–CO_3 LDHs were first characterized using XRD analysis, as shown in Fig. 2(a). Six characteristic peaks which can be indexed to the reflections of (003), (006), (009), (015), (018), and (110/113) planes were observed for the LDHs, suggesting that all of the LDHs had a well-developed layer structure. The basal spacing of flower-like, spherical, and plate-like Mg_3Al–CO_3 LDHs was determined to be 7.88, 7.80, and 7.77 nm, respectively. Fig. 2(a) shows that the peak intensity of XRD reflections follows the order of plate-like > spherical > flower-like LDHs, suggesting that the crystallinity degree also follows the order of plate-like > spherical > flower-like LDHs. This is consistent with the basal spacing of LDHs, which indicates that higher crystallinity degree will lead to narrower layer distance. For the plate-like LDH that was synthesized using hydrothermal method at 150 °C, a very weak peak at *ca.* 29.4° was observed, which can be indexed to the impurity of $Mg_2CO_3(OH)_2 \cdot 3H_2O$ (PDF 06-0484). The formation of this impurity phase might be due to the relatively high synthesis temperature and pressure, the basic condition (pH = 12), and long synthesis time (3 days).

The morphology of synthesized LDHs was characterized using both SEM and TEM analyses. The SEM images in Fig. 2(b–d) clearly indicate that LDHs with three different types of morphology including spherical nanoparticle, plate-like, and flower-like shaped particles were successfully synthesized. The average particle size of the spherical LDH is only *ca.* 30 nm. However, due to the high surface charge and tension, these nanoparticles aggregated severely after being dried. The plate-like LDH particles are quite even, with an average lateral size of *ca.* 300 nm. The flower-like LDH particles have an average size of approximately 400 nm. The thickness of the "petals" is about 24–25 nm, which accounts for about 30 brucite-like sheets. Comparing to the dried spherical LDH, although the aggregation of the dried plate-like and flower-like LDHs was relatively less, it is still a problem for obtaining well dispersed LDHs within the polymer matrix. Thus, in order to prevent the

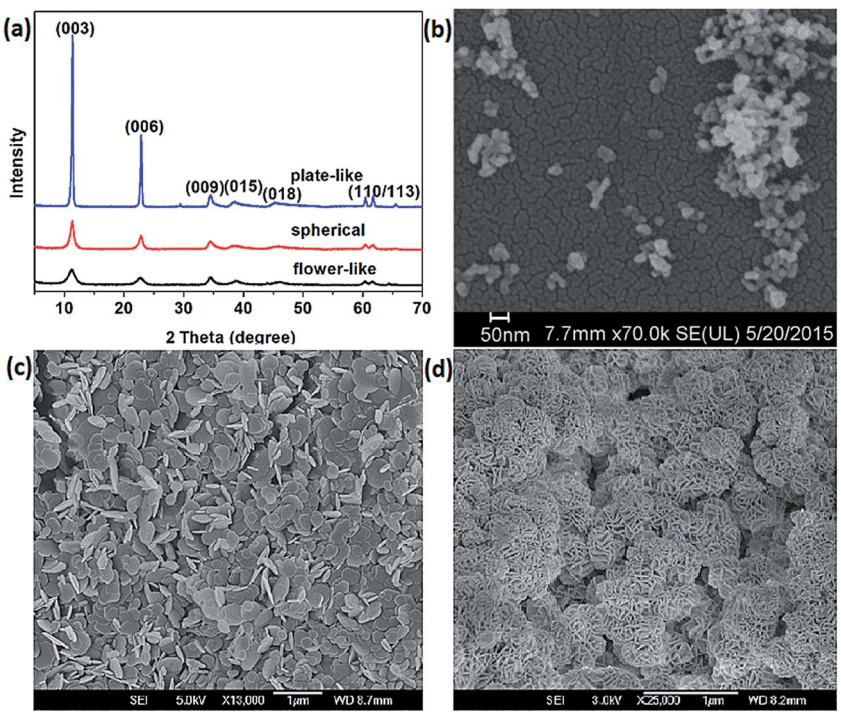

Fig. 2 XRD patterns of (a) spherical, plate-like, and flower-like Mg_3Al–CO_3 LDHs and SEM images of (b) spherical, (c) plate-like, and (d) flower-like Mg_3Al–CO_3 LDHs.

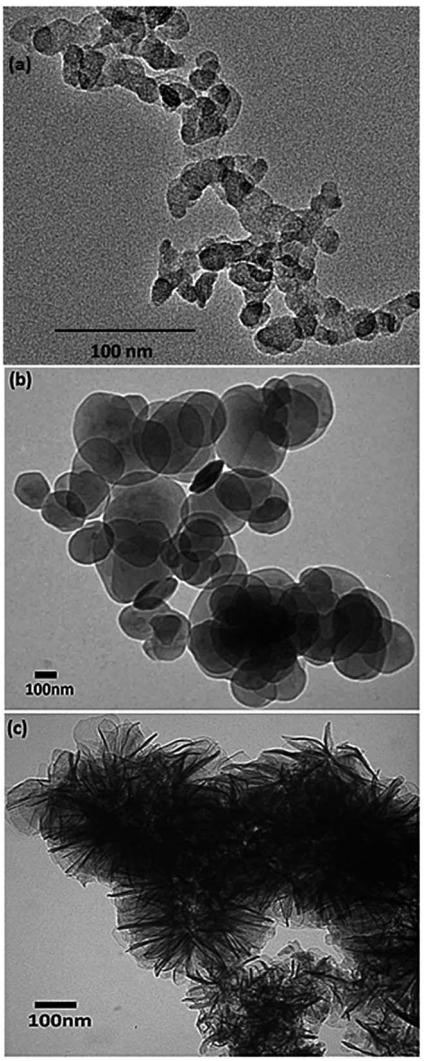

Fig. 3 TEM images of (a) spherical, (b) plate-like, and (c) flower-like $Mg_3Al–CO_3$ LDHs.

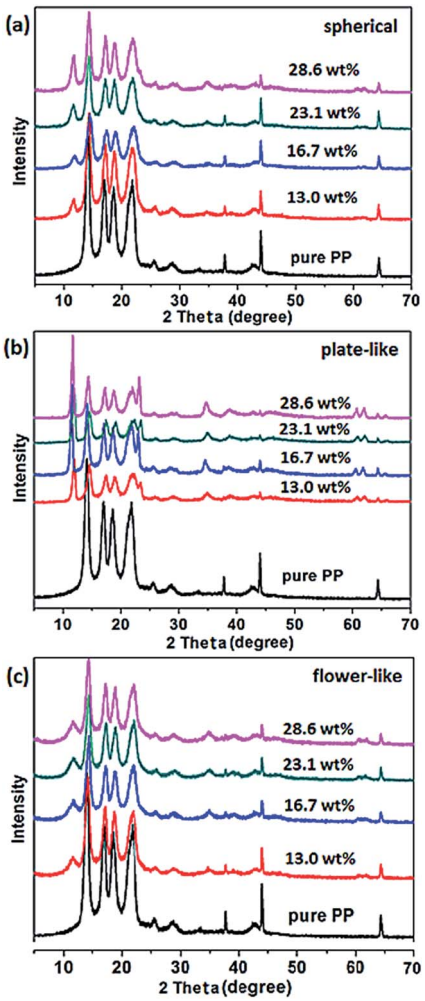

Fig. 4 XRD patterns of (a) PP/spherical LDH nanocomposites, (b) PP/plate-like LDH nanocomposites, and (c) PP/flower-like LDH nanocomposites.

aggregation of nanoparticles, LDHs were washed with acetone intensively and introduced into polymers before any drying step. Fig. 3 shows the TEM images of the obtained three types of LDHs, in which the difference among the nanoparticles was more distinguishable. The fine control of the morphology of LDHs is one the key prerequisites for the present work. For this purpose, the synthesis pH, temperature, and pressure are crucial for the growth of LDH nanoparticles. The detailed formation mechanism can be found in our previous report.[18] Due to their morphological features of these three types of LDHs, the spherical, plate-like, and flower-like LDHs can be referred as 0-dimensional, 2-dimensional, and 3-dimensional nanoparticles, respectively. In this contribution, we systematically investigated how such difference in morphology affects the thermal, flame retardant, and rheological behaviors of PP nanocomposites.

After adding the LDH nanofillers into PP, the obtained nanocomposites were first characterized using XRD analysis. Fig. 4 shows the XRD patterns of pure PP and PP/$Mg_3Al–CO_3$ LDH nanocomposites with the LDH loading of 13.0, 16.7, 23.1, and 28.6 wt%, respectively. The characteristic XRD patterns of LDHs were clearly seen, especially for the (003) diffraction peak. For all three types of LDHs, the intensity increased with increasing LDH loading, indicating that LDH nanoparticles were successfully introduced into PP using the solvent mixing method.

The morphology of synthesized nanocomposites and the distribution of LDH nanoparticles were further examined by SEM analysis. Fig. 5 presents the SEM images of PP/$Mg_3Al–CO_3$ LDH nanocomposites with the LDH loading of 13.0 and 28.6 wt%, respectively. Although the solvent mixing method can lead to a better LDH dispersion within PP, some bulk LDH particles were still observed on the surface of PP nanocomposites. With increasing the LDH loading, the size of these particles remains practically unchanged, only their amount increased. Fig. 6 shows the SEM images of three types of PP/LDH nanocomposites with higher magnifications. The spherical, plate-like, and flower-like nanoparticles were clearly seen in their corresponding nanocomposites, suggesting that the morphology of LDHs kept unchanged after being added into PP.

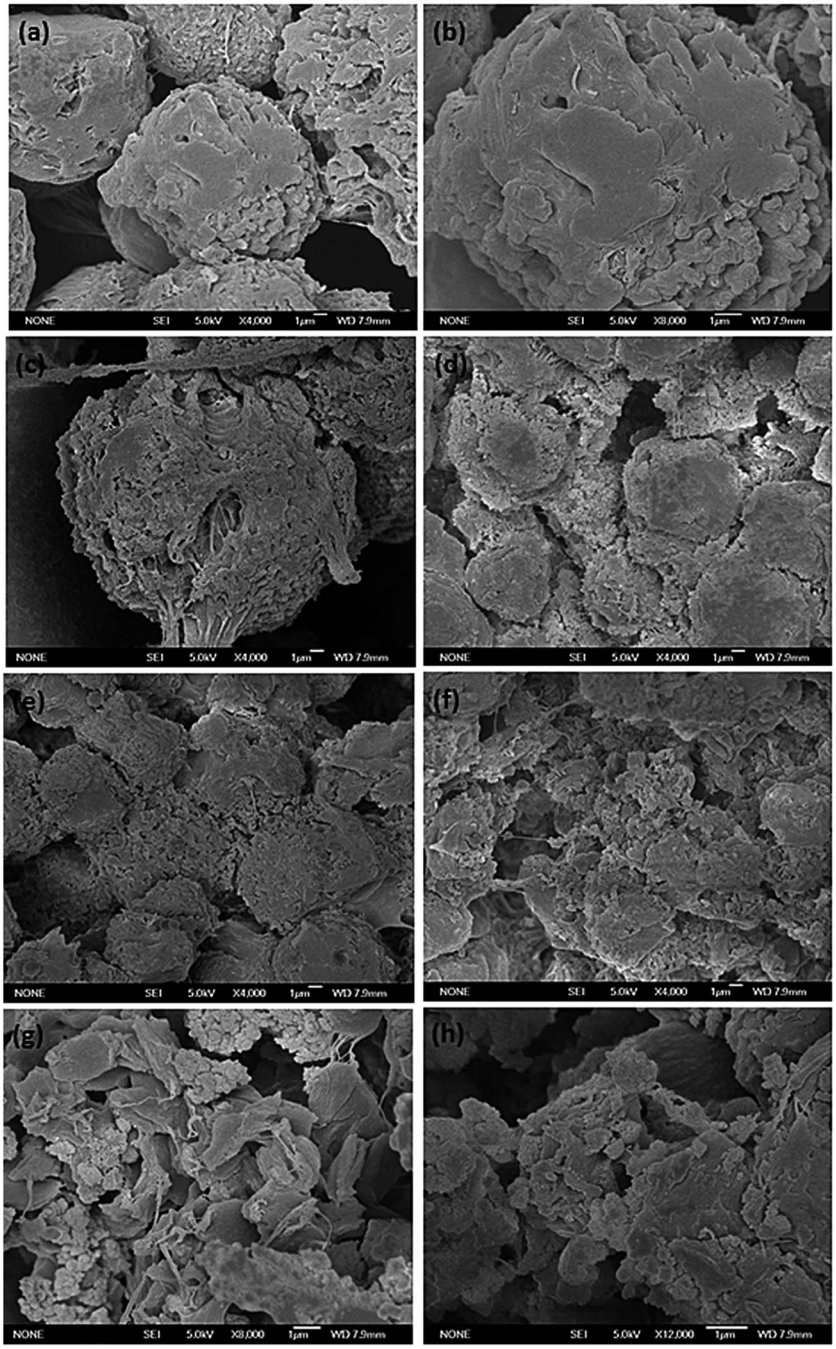

Fig. 5 SEM images of (a) pure PP × 4000, (b) pure PP × 8000, (c and d) PP/spherical LDH nanocomposites with a loading of 13.0 and 28.6 wt%, (e and f) PP/plate-like LDH nanocomposites with a loading of 13.0 and 28.6 wt%, and (g and h) PP/flower-like LDH nanocomposites with a loading of 13.0 and 28.6 wt%.

3.2 Performance test of PP/LDH nanocomposites

Since LDH nanofillers may affect the thermal stability of PP, the influence of the morphology of LDHs on the thermal stability of PP was studied by TGA, as shown in Fig. 7 and Table 1. For evaluating the thermal stability of polymeric materials using TGA analysis, usually two typical temperatures are of great importance. One is the onset of decomposition temperature ($T_{0.1}$) at which 10% weight loss takes place and the other is the decomposition temperature ($T_{0.5}$) at which 50% weight loss takes place. The weight loss was observed to start at about 270 °C for all samples. The $T_{0.5}$ of pure PP was 331 °C. However, after incorporating LDH nanoparticles, the $T_{0.5}$ of majority of PP/LDH nanocomposites was increased significantly. It is obvious that the addition of Mg_3Al–CO_3 LDHs to PP significantly improves the thermal stability of PP, particularly when the LDH loading is not very high. For example, the $T_{0.1}$ of pure PP was 280 °C, while the $T_{0.1}$ of PP/LDH nanocomposites with a

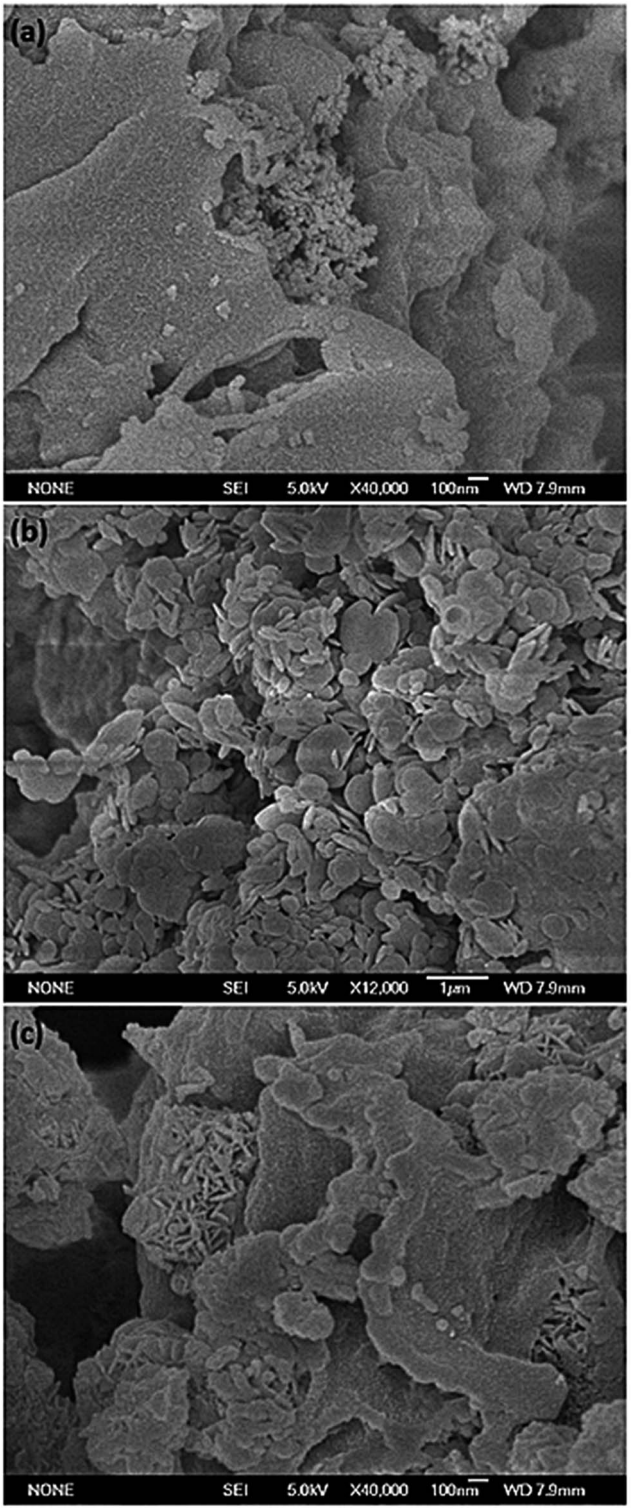

Fig. 6 SEM images of (a) spherical PP/LDH nanocomposites with 13.0 wt% LDH loading, (b) plate-like PP/LDH nanocomposite with 28.6 wt% LDH loading, and (c) flower-like PP/LDH nanocomposite with 28.6 wt% LDH loading.

LDH loading of only 13.0 wt% was increased to 318, 315, and 315 °C for spherical, plate-like, and flower-like LDHs, increased by 38, 35, and 35 °C, respectively. And with 13.0 wt% of LDH, the $T_{0.5}$ of PP/LDH nanocomposites was significantly increased by 52, 61, and 49 °C for spherical, plate-like, and flower-like LDHs, respectively. However, when the LDH loading was high (>13.0 wt%), the $T_{0.5}$ started to decrease with the increase in LDH loading. This is probably because the LDH as a weak alkaline can catalyze the degradation of PP due to the presence of hydroxyl groups. When the LDH loading is low (13 wt%), the nanoscale-dispersed Mg_3Al-LDH in PP matrix produces good obstruct effect for the escape of degraded low molecules and thus overcomes itself negative catalytic degradation effect on PP. While when the LDH loading is high, the negative catalytic degradation effect increased with the increase in LDH loading, leading to a relatively worse thermal stability of PP/LDH nanocomposites. This data is also consistent with literature reports.[45–47] Fig. 7(d) summarizes the effects of the morphology and loading of LDHs, which clearly shows that plate-like LDH led to a better thermal stability. This data demonstrated that the influence of LDH morphology on thermal stability follows the order of plate-like > spherical > flower-like.

MCC measures the flammability of materials on milligram quantities and is based on the principle of oxygen consumption. It is a small-scale flammability testing technique to screen polymer flammability prior to scale-up and is a convenient, fast, and relatively new technique for laboratory evaluation of the flame properties. It was regarded as one of the most effective methods for investigating the combustion properties of polymer materials.[48–50] In the case of MCC measurement, the heat is produced *via* full combustion of the fuel gases generated during the pyrolysis of samples, showing several parameters, such as specific heat release rate (HRR), heat release capacity (HRC), total heat release (THR), *etc.* These parameters are very important to reflect the combustion properties of materials and allow a reasonable estimation of the fire hazard using small quantities of samples.[39]

The HRR plots of PP and its nanocomposites are shown in Fig. 8 and the corresponding combustion data are presented in Table 2. It is obvious that the peak heat release rate (PHRR) values of all PP/Mg_3Al–CO_3 LDH nanocomposites were much lower than that of pure PP. For all the PP/LDH nanocomposites, the reduction in PHRR increased with the increase in LDH loading. For pure PP, the PHRR value was 1640 W g^{-1}. After adding LDHs, the PHRR value of PP/spherical LDH nanocomposites was reduced by 29.8, 37.4, 44.2, and 57.9% with 13.0, 16.7, 23.1, and 28.6 wt% LDH loading, respectively. For the PP/flower-like LDH nanocomposites, the PHRR value was reduced by 26.7, 29.3, 40.2, and 54.8% with 13.0, 16.7, 23.1, and 28.6 wt% LDH loading, respectively. Among these three types of nanocomposites, PP/plate-like LDH nanocomposites showed relatively better flame retardant performance. After adding 13.0, 16.7, 23.1, and 28.6 wt% LDH, the PHRR value of the nanocomposites was reduced by 33.2, 36.3, 44.4, and 60.7%, respectively. These results clearly indicate that the Mg_3Al–CO_3 LDHs can significantly improve the flame retardant performance of PP. Also, LDHs with different morphology have different flame retardant efficiency, which follows the order of plate-like > spherical > flower-like. These results are in good agreement with the thermal stability.

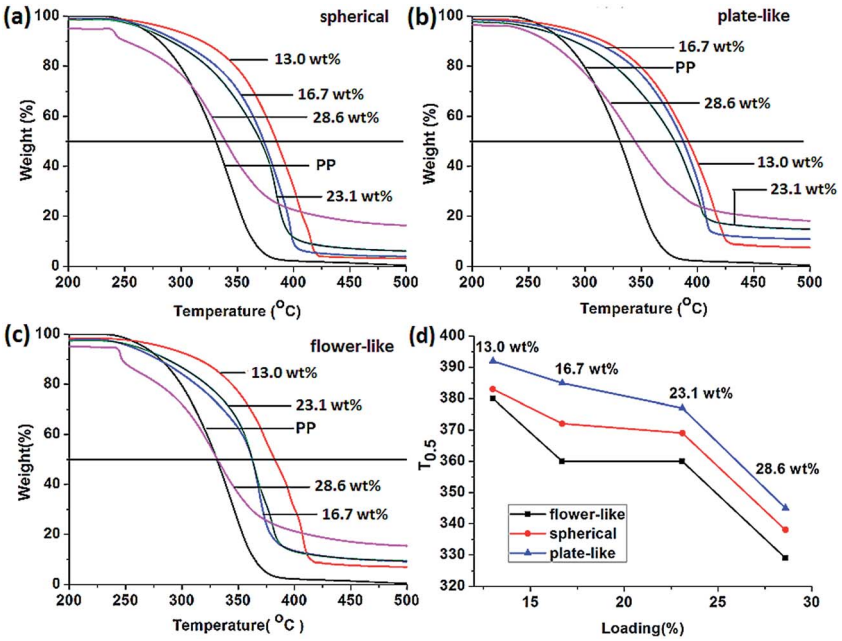

Fig. 7 TGA analysis of (a) PP/spherical LDH nanocomposites, (b) PP/plate-like LDH nanocomposites, (c) PP/flower-like LDH nanocomposites, and (d) graph of $T_{0.5}$ *vs.* LDH loading.

The HRC is another important parameter usually used to predict and evaluate the fire hazard. The HRC values obtained as a sum of all PHRR values are summarized in Table 2 as well. Pure PP exhibited the highest HRC of 1170 J g^{-1} K^{-1}. After adding LDHs, this value was decreased obviously with increasing the LDH loading. For instance, with 13.0, 16.7, 23.1, and 28.6 wt% plate-like LDHs, the HRC of the nanocomposites was decreased to 834, 796, 887, and 862 J g^{-1} K^{-1}, respectively. Similar to the HRR results, the influence of morphology on HRC also follows the order of plate-like > flower-like > spherical.

THR is another important parameter for fire hazard evaluation. Once the ignition happens, THR steadily increased with burning time and attained a steady state before the flameout occurs. Consequently, the reduction in THR of PP/LDH nanocomposites could be an evaluation for these efficient flame retardant fillers. According to Table 2, THR was reduced with the increase in LDH loading for all types of LDHs. Comparing to the THR value of 47.4 kJ g^{-1} for pure PP, with a LDH loading of 13.0, 16.7, 23.1, and 28.6 wt%, PP/spherical LDH nanocomposites showed a THR value of 41.6, 41.1, 43.3, and 31.8 kJ g^{-1}, PP/plate-like LDH nanocomposites showed a THR value of 39.0, 37.8, 36.0, and 30.9 kJ g^{-1}, and PP/flower-like LDH nanocomposites showed a THR value of 37.9, 40.3, 36.8, and 32.7 kJ g^{-1}, respectively. Similar to the HRR and HRC results, the THR was also significantly reduced after adding LDHs. And the influence of morphology on THR of the PP/LDH nanocomposites flows the order of plate-like > flower-like > spherical. All the above results suggested that Mg_3Al–CO_3 LDHs are highly efficient flame retardant nanofillers and the morphology was demonstrated to be one of the important influencing factors.

Table 1 Summary of TGA results of pure PP and its nanocomposites[a]

Sample	$T_{0.1}$/°C	$\Delta T_{0.1}$/°C	$T_{0.5}$/°C	$\Delta T_{0.5}$/°C
PP	280	NA	331	NA
PP/13.0 wt% spherical	318	38	383	52
PP/16.7 wt% spherical	296	16	372	41
PP/23.1 wt% spherical	291	11	369	38
PP/28.6 wt% spherical	250	−30	338	7
PP/13.0 wt% plate-like	315	35	392	61
PP/16.7 wt% plate-like	305	25	385	54
PP/23.1 wt% plate-like	290	10	377	46
PP/28.6 wt% plate-like	266	−14	345	14
PP/13.0 wt% flower-like	315	35	380	49
PP/16.7 wt% flower-like	278	−2	360	29
PP/23.1 wt% flower-like	285	5	360	29
PP/28.6 wt% flower-like	246	−34	329	−2

[a] $T_{0.1}$ = temperature of 10% mass loss; $T_{0.5}$ = temperature of 50% mass loss; ΔT = difference between virgin polymer and its nanocomposites.

The rheological behaviors of the polymer nanocomposites melts are very important for industrial processing.[51] The behaviors can be detected by characterizing the storage modulus (G') and loss modulus (G'') as a function of frequency.[52–54] Fig. 9 and 10 show the G' and G'' as a function of frequency for pure PP and its nanocomposites melts. Within the experimental frequency range, the G' of pure PP was found to be lower than its G''. This means that the viscous component has a dominant effect on the flow behavior of pure PP melt in this frequency range. With increasing frequency, the G' increased more than the G'' indicating increasing contribution of the elastic response. This is a typical behavior of unfilled thermoplastic melt.[55] On the contrary, in PP/LDH nanocomposites, G' always remains higher than G'' within the experimental frequency range indicating dominant elastic character of the

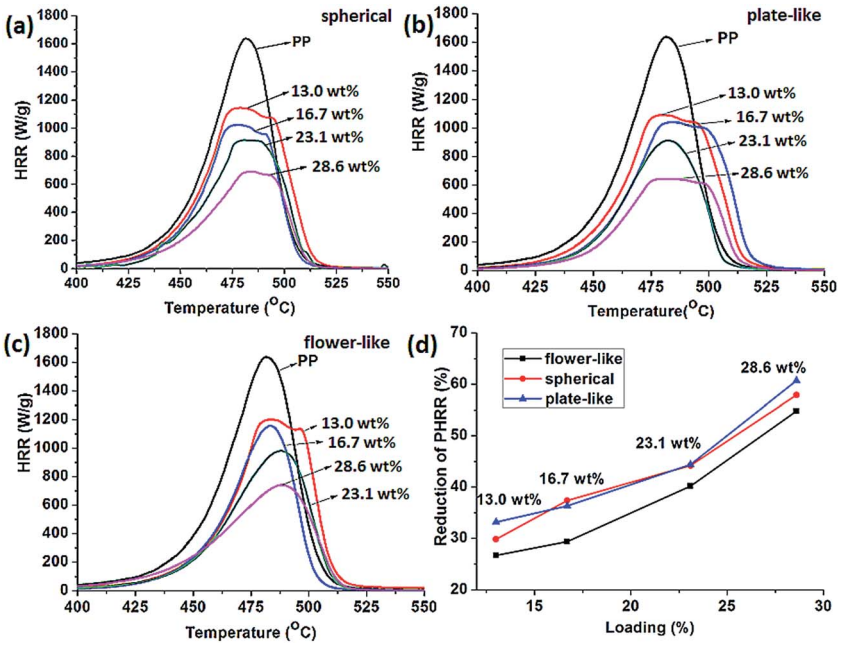

Fig. 8 MCC analysis of (a) PP/spherical LDH nanocomposites, (b) PP/plate-like LDH nanocomposites, (c) PP/flower-like LDH nanocomposites, and (d) PHRR reduction of PP/LDH nanocomposites *vs.* LDH loading.

material.[56] In general, both G' and G'' of PP increased after introducing Mg_3Al–CO_3 LDHs. Furthermore, both of them increased with the increase in LDH loading, particularly at low frequencies, which results from a high surface friction of the PP/LDH interlayer. The influence of morphology on G' and G'' follows the order of spherical > plate-like > flower-like, suggesting that different morphologies could result in different rheological behaviors. One interesting phenomenon is that the influence of morphology on G' and G'' shares some similarities to the influence on flame retardancy. In other words, the influence of morphology on G' and G'' of PP/flower-like LDH nanocomposites was weaker than the other two, although the intrinsic reason for such correlation is still unclear so far.

Fig. 11 shows the mechanical loss factor (tan δ) as a function of frequency, tan δ is the ratio of loss modulus to storage modulus, which is highly related to the applied frequency. With the spherical and plate-like LDHs as nanofillers, tan δ first decreased with the increase in LDH loading from 13.0 to 23.1 wt% and then started to increase slightly with 28.6 wt% LDH. While with the flower-like LDHs as nanofillers, tan δ decreased with the increase in LDH loading. The tan δ of all the nanocomposites shows three different stages: rubbery, viscoelastic, and glassy states.[57] It was reported that the incorporation of LDH nanoparticles restrains the relative motion of polymer chain and makes the nanocomposites "stiffer".[34,51,57,58]

Table 2 Summary of MCC results of PP and its nanocomposites[a]

Sample	PHRR/W g^{-1}	Reduction/%	THR/kJ g^{-1}	T_{max}/°C	HRC/J g^{-1} K^{-1}
PP	1640	NA	47.4	478.6	1170
PP/13.0 wt% spherical	1151	29.8	41.6	496.6	1098
PP/16.7 wt% spherical	1027	37.4	41.1	475.5	1185
PP/23.1 wt% spherical	915	44.2	43.3	480.8	908
PP/28.6 wt% spherical	691	57.9	31.8	482.0	664
PP/13.0 wt% plate-like	1096	33.2	39.0	482.8	834
PP/16.7 wt% plate-like	1044	36.3	37.8	486.3	796
PP/23.1 wt% plate-like	912	44.4	36.0	479.9	887
PP/28.6 wt% plate-like	644	60.7	30.9	479.8	862
PP/13.0 wt% flower-like	1202	26.7	37.9	471.4	1090
PP/16.7 wt% flower-like	1159	29.3	40.3	479.9	1077
PP/23.1 wt% flower-like	981	40.2	36.8	482.8	842
PP/28.6 wt% flower-like	741	54.8	32.7	481.1	618

[a] HRC = heat release rate; THR = total heat release; PHRR = peak heat release rate; T_{max} = temperature at maximum pyrolysis rate.

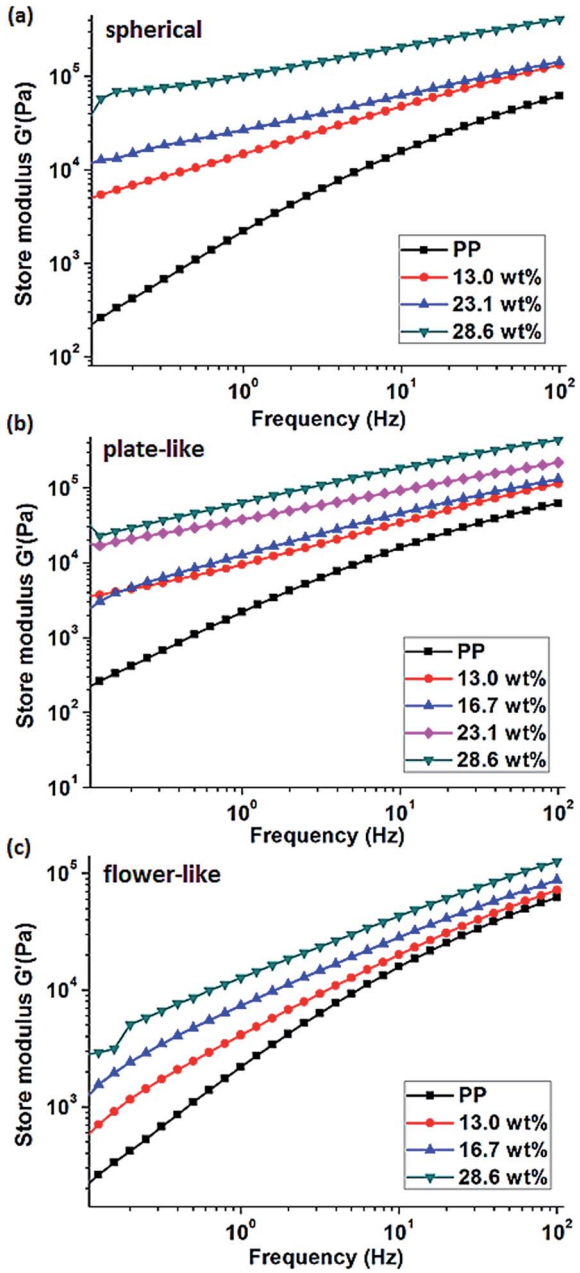

Fig. 9 Storage modulus (G') *vs.* frequency for (a) PP/spherical LDH nanocomposites, (b) PP/plate-like LDH nanocomposites, and (c) PP/flower-like LDH nanocomposites.

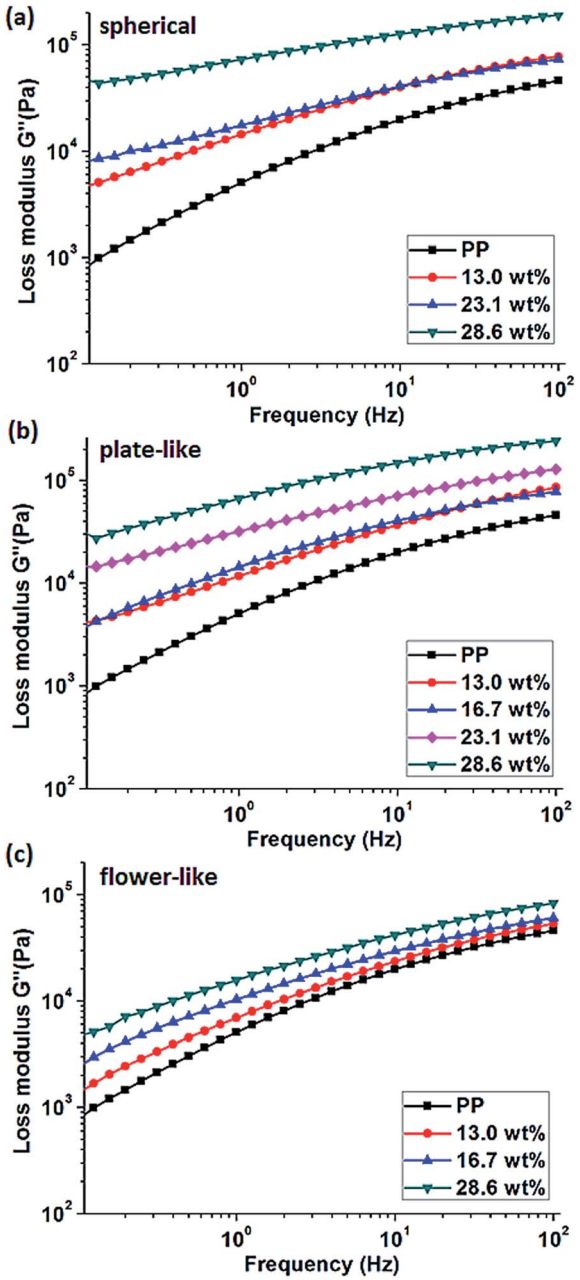

Fig. 10 Loss modulus (G'') *vs.* frequency for (a) PP/spherical LDH nanocomposites, (b) PP/plate-like LDH nanocomposites, and (c) PP/flower-like LDH nanocomposites.

Fig. 12 shows the complex viscosity (η^*) as a function of frequency for pure PP and its nanocomposite melts. $\eta^*(w)$ is strongly related to G' and G'' and can be calculated using eqn (1).

$$\eta^*(w) = [(G'/w)^2 + (G''w^2)]^{1/2} \quad (1)$$

The pure PP shows a classical viscoelastic behavior characterized by a transition from low frequency Newtonian flow behavior to a high frequency shear thinning nature (viscosity decreases with an increase of shear rate/frequency).[59,60] The η^* of all PP/LDH nanocomposite melts increased with the increase in LDH loadings from 0 to 28.6 wt%. And the influence of morphology on η^* flows the order of spherical > plate-like > flower-like. The increment of the melt viscosity was resulted from the stronger interaction between LDH with various LDH fillers and the PP matrix, indicating that LDH particles restrict the PP chain movements more significantly. For PP/spherical and PP/plate-like LDH nanocomposites, the viscosity curves become linear within the whole frequency range after adding LDHs. This phenomenon indicates the filler dominated fluid in the nanocomposites with 13.0, 16.7, 23.1, and 28.6 wt% LDH loadings. The transition in η^* indicates that the

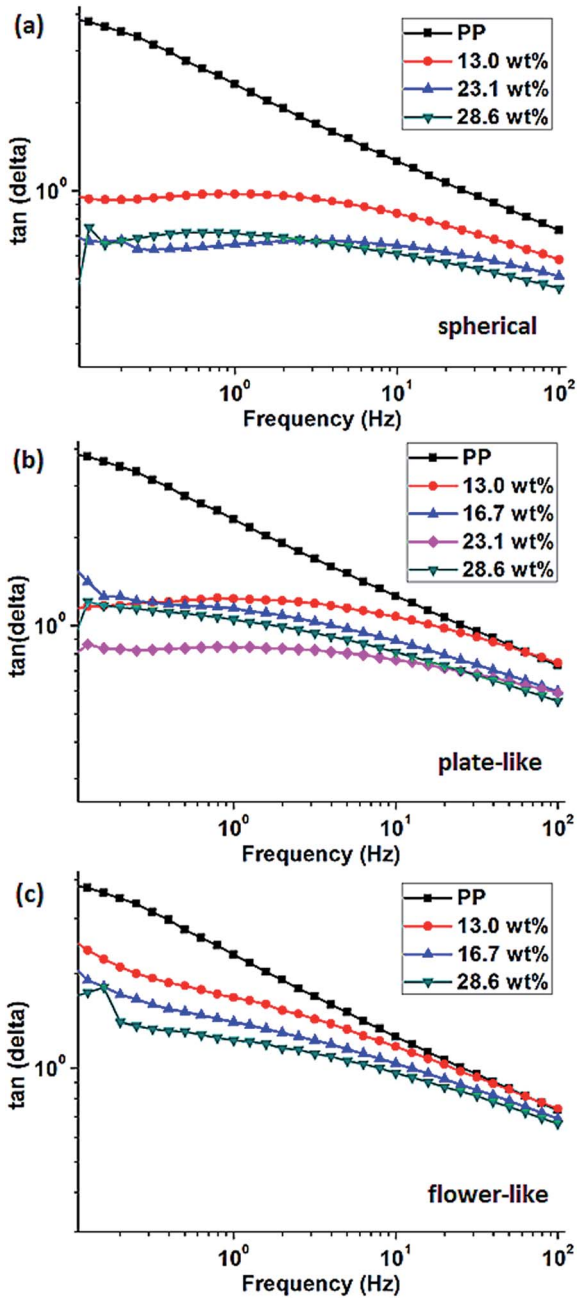

Fig. 11 tan δ *vs.* frequency for (a) PP/spherical LDH nanocomposites, (b) PP/plate-like LDH nanocomposites, and (c) PP/flower-like LDH nanocomposites.

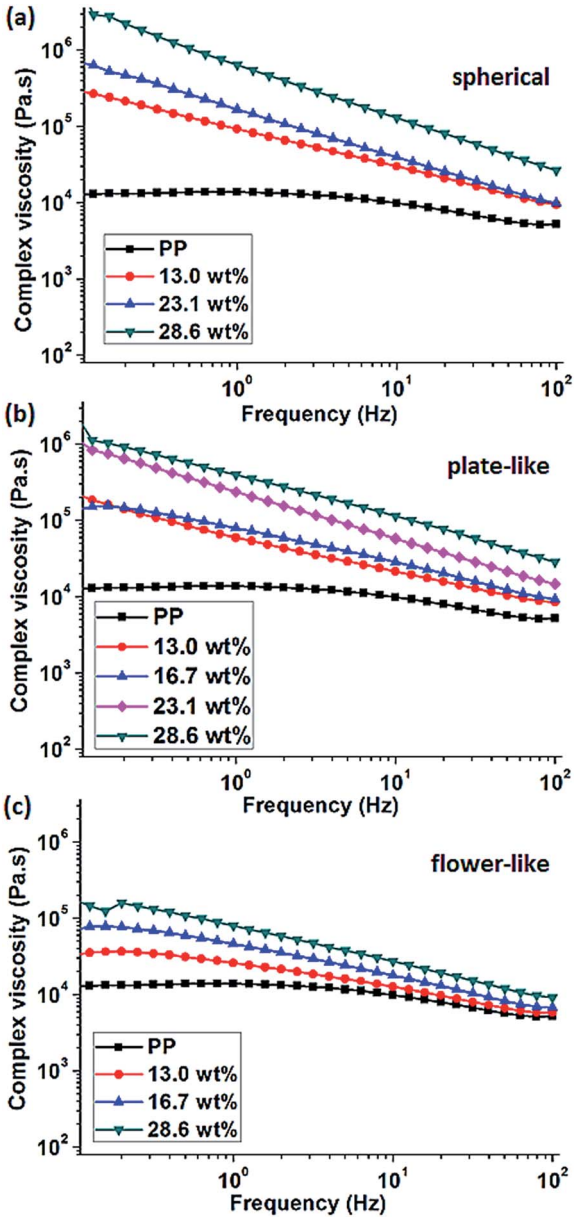

Fig. 12 Complex viscosity *vs.* frequency for (a) PP/spherical LDH nanocomposites, (b) PP/plate-like LDH nanocomposites, and (c) PP/flower-like LDH nanocomposites.

nanocomposites have reached a rheological percolation, at which the nanoparticles form a network structure and greatly impede the motion of the polymer chains.[61]

In summary, we have demonstrated that the morphology of LDHs has a big effect on the thermal stability, flame retardancy, and rheological property of PP nanocomposites. Considering that all LDHs have a similar layered structure and chemical composition, the intrinsic reason for the difference caused by the morphology is still under investigation. One possible explanation might be that the different morphologies give slightly different LDH particle sizes and size distributions, which dominates the physical and mechanical performance of the PP/LDH nanocomposites.

4. Conclusion

In this contribution, we investigated the influence of three types of Mg_3Al–CO_3 LDHs (spherical, plate-like, and flower-like) as nanofillers on the thermal stability, flame retardancy performance, and rheological behaviors of PP nanocomposites for the first time. The obtained PP/LDH nanocomposites showed significantly improved thermal stability and fire retardant performance compared to neat PP. TGA analysis indicated that

the $T_{0.5}$ of 13.0 wt% PP/plate-like LDH nanocomposites was dramatically increased by 61 °C compared to that of pure PP. MCC analysis confirmed that the flame retardant efficiency was dependent on both the morphology and the loading of LDHs. With 28.6 wt% LDH, the PHRR reduction for PP/flower-like, PP/spherical, and PP/plate-like LDH nanocomposites was 54.8%, 57.9%, and 60.7%, respectively. The influence of LDH morphology on the efficiency of flame retardancy was observed to follow the order of plate-like > spherical > flower-like. Moreover, the influence on G' and G'' was observed to follow the order of spherical > plate-like > flower-like. The thermal stability, flame retardancy, and rheological behaviors of PP/LDH nanocomposites were demonstrated to be highly dependent on LDH morphology. Thus, for practical applications of these kinds of nanocomposites, a proper selection of the morphology and loading of LDHs should be considered.

Acknowledgements

This work is supported by the Fundamental Research Funds for the Central Universities (TD-JC-2013-3 and BLYJ201402), the Beijing Nova Programme (Z131109000413013), the Program for New Century Excellent Talents in University (NCET-12-0787), the National Natural Science Foundation of China (51308045), and the Project Sponsored by the Scientific Research Foundation for the Returned Overseas Chinese Scholars, State Education Ministry.

References

1 L. Wang, X. He, H. Lu, J. Feng, X. Xie, S. Su and C. A. Wilkie, *Polym. Adv. Technol.*, 2011, **22**, 1131.
2 K. L. Edwards, *Mater. Des.*, 2004, **25**, 529.
3 L. Sun, J. Liu, S. R. Kirumakki, E. D. Schwerdtfeger, R. J. Howell, K. Al Bahily, S. A. Miller, A. Clearfield and H. Sue, *Chem. Mater.*, 2009, **21**, 1154.
4 J. Zhu, Q. He, Z. Luo, A. Khasanov, Y. Li, L. Sun, Q. Wang, S. Wei and Z. Guo, *J. Mater. Chem.*, 2012, **22**, 15928.
5 J. Kaspersma, C. Doumen, S. Munro and A. M. Prins, *Polym. Degrad. Stab.*, 2002, **77**, 325.
6 M. Yamaguchi, H. Miyata and K. Nitta, *J. Appl. Polym. Sci.*, 1996, **62**, 87.
7 Q. Wang, X. Zhang, J. Zhu, Z. Guo and D. O'Hare, *Chem. Commun.*, 2012, **48**, 7450.
8 A. B. Morgan, C. A. Wilkie, *Flame Retardant Polymer Nanocomposites*, John Wiley & Sons, Inc., 2007.
9 C. J. Hilado, *Flammability Handbook for Plastics*, CRC Press, 1998.
10 Y. Gao, J. Wu, Q. Wang, C. A. Wilkie and D. O'Hare, *J. Mater. Chem. A*, 2014, **2**, 10996.
11 L. Qiu, W. Chen and B. Qu, *Polym. Degrad. Stab.*, 2005, **87**, 433.
12 J. Liu, G. Chen and J. Yang, *Polymer*, 2008, **49**, 3923.
13 C. Nyambo, D. Chen, S. Su and C. A. Wilkie, *Polym. Degrad. Stab.*, 2009, **94**, 496.
14 Q. Wang and D. O'Hare, *Chem. Rev.*, 2012, **112**, 4124.
15 Q. Wang, S. V. Y. Tang, E. Lestercd and D. O'Hare, *Nanoscale*, 2013, **5**, 114.
16 Q. Wang, H. H. Tay, D. J. Wei, L. Chen, Y. Liu, J. Chang, Z. Zhong, J. Luo and A. Borgna, *ChemSusChem*, 2010, **3**, 965.
17 Q. Wang, Y. Gao, J. Luo, Z. Zhong, A. Borgna, Z. Guo and D. O'Hare, *RSC Adv.*, 2013, **3**, 3414.
18 Q. Wang, H. H. Tay, Z. Guo, L. Chen, Y. Liu, J. Chang, Z. Zhong, J. Luo and A. Borgna, *Appl. Clay Sci.*, 2012, **55**, 18.
19 Q. Wang, J. Yu, J. Liu, Z. Guo, A. Umar and L. Sun, *Sci. Adv. Mater.*, 2013, **5**, 469.
20 Q. Wang, Y. Gao, Z. Zhang, L. Duan, A. Umar and D. O'Hare, *Sci. Adv. Mater.*, 2013, **5**, 411.
21 V. Rives, *Layered Double Hydroxides: Present and Future*, Nova Publishers, 2001.
22 Y. Zhao, M. Wei, J. Lu, Z. Wang and X. Duan, *ACS Nano*, 2009, **3**, 4009.
23 Y. Lin, D. Li, D. G. Evans and X. Duan, *Polym. Degrad. Stab.*, 2005, **88**, 286.
24 Z. Xu, S. K. Saha, P. S. Braterman and N. D. Souza, *Polym. Degrad. Stab.*, 2006, **91**, 3237.
25 D. G. Evans and X. Duan, *Chem. Commun.*, 2006, **5**, 485.
26 Q. Wang, H. H. Tay, L. Chen, Y. Liu, J. Chang, Z. Zhong, J. Luo and A. Borgna, *J. Nanoeng. Nanomanuf.*, 2011, **1**, 298.
27 D. Li, Z. Tuo, D. G. Evans and X. Duan, *J. Solid State Chem.*, 2006, **179**, 3114.
28 Y. Feng, D. Li, Y. Wang, D. G. Evans and X. Duan, *Polym. Degrad. Stab.*, 2006, **91**, 789.
29 X. Zhao, F. Zhang, S. Xu, D. G. Evans and X. Duan, *Chem. Mater.*, 2010, **22**, 3933.
30 C. Jiao, Z. Wang, X. Chen and Y. Hu, *J. Appl. Polym. Sci.*, 2008, **107**, 2626.
31 F. R. Costa, U. Wagenknecht and G. Heinrich, *Polym. Degrad. Stab.*, 2007, **92**, 1813.
32 Z. Cui and B. Qu, *Chin. J. Polym. Sci.*, 2010, **28**, 563.
33 L. Du and B. Qu, *J. Mater. Chem.*, 2006, **16**, 1549.
34 Q. Wang, X. Zhang, C. Wang, J. Zhu, Z. Guo and D. O'Hare, *J. Mater. Chem.*, 2012, **22**, 19113.
35 F. R. Costa, U. Wagenknecht and G. Heinrich, *Polym. Degrad. Stab.*, 2007, **92**, 1813.
36 C. Nyambo, P. Songtipya, E. Manias, M. M. Jimenez-Gasco and C. A. Wilkie, *J. Mater. Chem.*, 2008, **18**, 4827.
37 C. M. Becker, A. D. Gabbardo, F. Wypych and S. C. Amico, *Composites, Part A*, 2011, **42**, 196.
38 W. Chen and B. Qu, *J. Mater. Chem.*, 2004, **14**, 1705.
39 D. Wang, A. Leuteritz, Y. Wang, U. Wagenknecht and G. Heinrich, *Polym. Degrad. Stab.*, 2010, **95**, 2474.
40 L. Shi, V. Li, S. Li, J. Wang, D. G. Evans and X. Duan, *Chin. Sci. Bull.*, 2005, **53**, 294.
41 S. Xu, L. Zhang, Y. Lin, R. Li and F. Zhang, *J. Phys. Chem. Solids*, 2012, **73**, 1514.
42 Y. Gao, J. Wu, Z. Zhang, R. Jin, X. Zhang, X. Yan, A. Umar, Z. Guo and Q. Wang, *J. Mater. Chem. A*, 2013, **1**, 9928.
43 Y. Gao, Q. Wang, J. Wang, L. Huang, X. Yan, X. Zhang, Q. He, Z. Xing and Z. Guo, *ACS Appl. Mater. Interfaces*, 2014, **6**, 5094.
44 Q. Wang, J. P. Undrell, Y. Gao, G. Cai, J. C. Buffet, C. A. Wilkie and D. O'Hare, *Macromolecules*, 2013, **46**, 6145.

45 L. Du, B. Qu, Y. Meng and Q. Zhu, *Compos. Sci. Technol.*, 2006, **66**, 913.
46 M. Zanetti, G. Camino, R. Thomann and R. Mulhaupt, *Polymer*, 2001, **42**, 4501.
47 A. Sorrentino, G. Gorrasi, M. Tortora, V. Vittoria, U. Costantino, F. Marmottini and F. Padella, *Polymer*, 2005, **46**, 1601.
48 B. Schartel, K. H. Pawlowski and R. E. Lyon, *Thermochim. Acta*, 2007, **462**, 1.
49 K. A. Ellzey, T. Ranganathan, J. Zilberman, E. B. Coughlin, R. J. Farris and T. Emrick, *Macromolecules*, 2006, **39**, 3553.
50 P. M. Hergenrother, C. M. Thompson, J. G. Smith, J. W. Connell, J. A. Hinkley, R. E. Lyon and R. Moulton, *Polymer*, 2005, **46**, 5012.
51 J. Zhu, S. Wei, Y. Li, L. Sun, N. Haldolaarachchige, D. P. Young, C. Southworth, A. Khasanov, Z. Luo and Z. Guo, *Macromolecules*, 2011, **44**, 4382.
52 J. Zhu, S. Wei, J. Ryu, M. Budhathoki, G. Liang and Z. Guo, *J. Mater. Chem.*, 2010, **20**, 4937.
53 J. Zhu, S. Wei, A. Yadav and Z. Guo, *Polymer*, 2010, **51**, 2643.
54 C. A. Mitchell, J. L. Bahr, S. Arepalli, J. M. Tour and R. Krishnamoorti, *Macromolecules*, 2002, **35**, 8825.
55 J. Ren, A. S. Silva and R. Krishnamoorti, *Macromolecules*, 2000, **33**, 3739.
56 S. P. Lonkar, S. Therias, F. Leroux, J. Gardette and R. P. Singh, *Polym. Eng. Sci.*, 2012, **52**, 2006.
57 X. Chen, S. Wei, A. Yadav, R. Patil, J. Zhu, R. Ximenes, L. Sun and Z. Guo, *Macromol. Mater. Eng.*, 2011, **296**, 434.
58 Y. Li, J. Zhu, S. Wei, J. Ryu, L. Sun and Z. Guo, *Macromol. Chem. Phys.*, 2011, **212**, 1951.
59 A. J. Poslinski, M. E. Ryan, R. K. Gupta, S. G. Seshadri and F. J. Frechette, *J. Rheol.*, 1988, **32**, 703.
60 V. M. Ugaz, D. K. Cinader and W. R. Burghardt, *Macromolecules*, 1997, **30**, 1527.
61 A. V. Shenoy, *Rheology of filled polymer systems*, Springer Science & Business Media, 1999.